

# Conversion of Methyl Mercaptan to Hydrocarbons over H-ZSM-5 Zeolite: DFT/BOMD Study

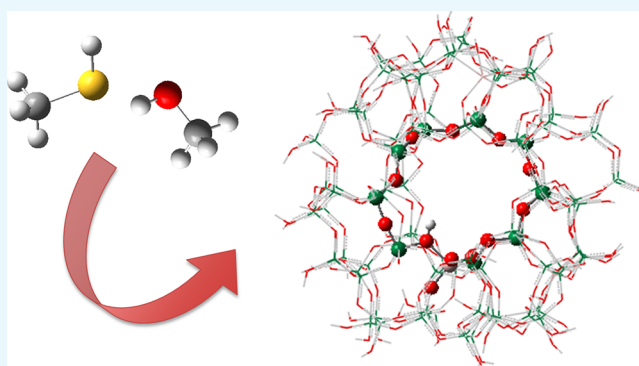
Miguel Reina,<sup>†,‡</sup> Ana Martínez,<sup>‡</sup> Claudia Cammarano,<sup>†</sup> Cathérine Leroi,<sup>§</sup> Vasile Hulea,<sup>†</sup> and Tzonka Mineva<sup>\*,†</sup>

<sup>†</sup>Institut Charles Gerhardt Montpellier, UMR 5253 CNRS/ENSCM/UM2/UM1, 8, rue de l'École Normale, 34296 Montpellier Cedex 5, France

<sup>‡</sup>Departamento de Materiales de Baja Dimensionalidad, Instituto de Investigaciones en Materiales, Universidad Nacional Autónoma de México, Circuito Exterior s/n, CU, P.O. Box 70-360, Coyoacán 04510, Ciudad de México, México

<sup>§</sup>TOTAL SA, Exploration & Production, 126, Avenue Larribau, 64018 Pau Cedex, France

**ABSTRACT:** Methyl mercaptan—a harmful impurity in natural gas—may be selectively converted into H<sub>2</sub>S and hydrocarbons [methyl mercaptan to hydrocarbon (M2TH) process], using zeolite catalysts. When M2TH is compared with the well-known MTH (methanol to hydrocarbons) process, significant differences emerge, essentially regarding the formation and distribution of products. Density functional theory (DFT) and Born–Oppenheimer molecular dynamics (BOMD) were employed to reveal possible origins for the experimentally observed differences. We established a close similarity between DFT intrinsic (electronic) reaction profiles in the stepwise mechanism of methanol and mercaptan dehydration, although no variance in reactivity was revealed. BOMD simulations at the experimental temperature of 823 K reveal rapid hydrogen abstraction from the methyl group in mercaptan, adsorbed in the zeolite cavity in the presence of the methoxy intermediate. The formation of •CH<sub>2</sub>SH radical is 10 times faster than that of •CH<sub>2</sub>OH at the same temperature. The varied reactivity of methanol and mercaptan in MTH and M2TH processes, respectively, can therefore first be attributed to very rapid hydrogen abstraction in mercaptan, which occurs in the zeolite cavity, following the formation of surface methoxy.



## INTRODUCTION

Methyl mercaptan (CH<sub>3</sub>SH) is invariably an abundant impurity in natural gas. For environmental and industrial reasons, its concentration should be maintained below 5 ppmv; however, CH<sub>3</sub>SH is one of the most refractory compounds to resist the gas cleanup process. Commercial procedures used to remove mercaptan from gas usually require formulated solvents or include reactions that need additional reagents that often generate waste. We have recently shown that CH<sub>3</sub>SH can be selectively transformed into hydrocarbons and H<sub>2</sub>S over H-zeolite/zeotypes with diverse topologies, for example, H-ZSM-5, H-Y, H-ferrierite, H-BEA, H-MOR, and H-SAPO-34.<sup>1,2</sup> The H<sub>2</sub>S produced can be efficiently captured by absorption using conventional solvents and made commercially saleable by applying the Claus process. The catalytic transformation of CH<sub>3</sub>SH was called M2TH (methyl mercaptan to hydrocarbons) and H-ZSM-5 was established as the most active and stable zeolite for this process.<sup>1</sup>

Methyl mercaptan is the sulfur analogue of methanol (CH<sub>3</sub>OH), whose conversion to hydrocarbons is known as methanol to hydrocarbons (MTH), representing a well-known industrial process.<sup>3</sup> To compare M2TH and MTH, the conversion of CH<sub>3</sub>OH and CH<sub>3</sub>SH under equivalent

conditions was investigated, using H-ZSM-5 zeolite as the catalyst.<sup>4</sup> Although similarities exist between M2TH and MTH, significant differences were observed, essentially regarding the catalyst lifetime and the formation of products. In the M2TH process, C1–C3 alkanes (with >90% of CH<sub>4</sub>) and benzene, toluene, and xylene (BTX) aromatics are the main hydrocarbons formed. Only a very small amount of olefins can be identified among the products. Similarly, in the few reports/patents dedicated to the methyl mercaptan conversion over microporous acid catalysts,<sup>5–7</sup> methane appears to be the main product obtained. In contrast, in the MTH process, products obtained are BTX aromatics and alkanes, but large amounts of C2–C4 olefins are also obtained.<sup>4</sup> In the MTH process, the catalyst also endured for longer than it did in the M2TH process.

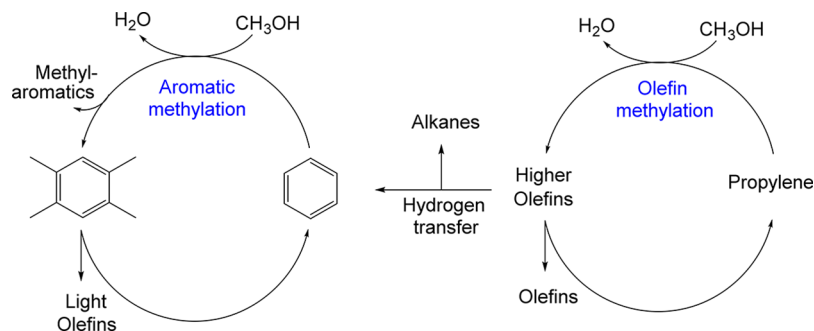
Generally, in the MTH process, the formation of lower olefins is assisted by the so-called “dual-cycle hydrocarbon pool” (HP) mechanism.<sup>8–12</sup> Accordingly, the aromatic hydrocarbons and olefins present inside the pores/cages of zeolites

Received: June 8, 2017

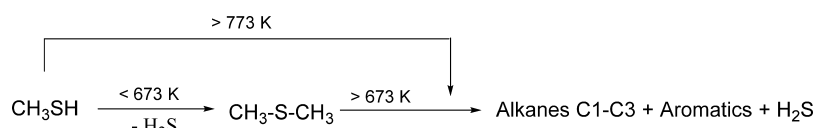
Accepted: August 3, 2017

Published: August 17, 2017

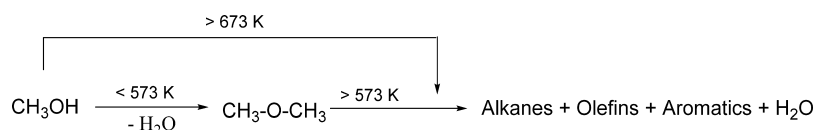
Scheme 1. “Dual-Cycle” Mechanism in the MTH Process (Adapted from Ref 11)



Scheme 2. Methyl Mercaptan Conversion over H-ZSM-5 Zeolite (According to Ref 1)



Scheme 3. Methanol Conversion over H-ZSM-5 (According to Ref 25)



undergo successive methylation steps by methanol, thus eliminating further olefins (Scheme 1).<sup>3,12</sup>

A similar mechanism has been proposed to explain the formation of olefins, when other C1 functionalized molecules, such as methyl halides ( $\text{CH}_3\text{X}$ ,  $\text{X} = \text{Cl}, \text{Br}, \text{I}$ ), were converted into hydrocarbons over zeolites ( $\text{CH}_3\text{X} \rightarrow \text{hydrocarbons} + \text{HX}$ ).<sup>13–15</sup> A general consensus opines that methylations represent key reaction stages in all these processes. Methanol and methyl halides are known to be efficient methylating agents.<sup>16–21</sup> Contrastingly, there is no information in the literature that demonstrates the capability of methyl mercaptan to methylate aromatics/olefins. The absence of olefins in the M2TH process suggests that the HP mechanism (based on methylation steps) is not sustained. Notably, only few theoretical studies have focused on adsorption<sup>22,23</sup> and conversion<sup>24</sup> of methyl mercaptan on acid zeolites. The most representative is the very recent density functional theory (DFT) study that describes the catalytic  $\text{CH}_3\text{SH}$  coupling over chabazite catalyst to form the C–C bond in ethylene.<sup>24</sup>

We investigated methylation by methyl mercaptan over the H-ZSM-5 catalyst for the first time, using Born–Oppenheimer molecular dynamics (BOMD) in conjunction with methods based on the quantum chemical DFT, to gain more insights into the mechanism of the zeolite-catalyzed M2TH process. We compared our results to those obtained from the methylation reaction with methanol, studied using the same computational methods and models. This report is organized as follows: first, we describe the zeolite models and computational methods used, subsequently we provide an overview of the experimental and theoretical results related to M2TH and MTH processes, and in the following sections, we present and discuss the intrinsic potential energy surface (PES) of dehydration reaction and the BOMD simulation at  $T = 823 \text{ K}$ .

## RESULTS AND DISCUSSION

**M2TH versus MTH—Overview of the Experimental Results.** The experimental studies related to the comparison between M2TH and MTH processes demonstrated that  $\text{CH}_3\text{SH}$  can be successfully converted over protonic zeolites (H-ZSM-5, H-Y, and H-ferrierite), without adding any reagent.<sup>1</sup> Below 673 K,  $\text{CH}_3\text{SH}$  is converted at equilibrium into dimethyl sulfide (DMS) and  $\text{H}_2\text{S}$ , and above 773 K, it is selectively converted into  $\text{H}_2\text{S}$  and hydrocarbons (essentially light alkanes and aromatics) (see Scheme 2).

The conversion of methanol over zeolites is known to follow analogous pathways (see Scheme 3).<sup>10,25</sup>

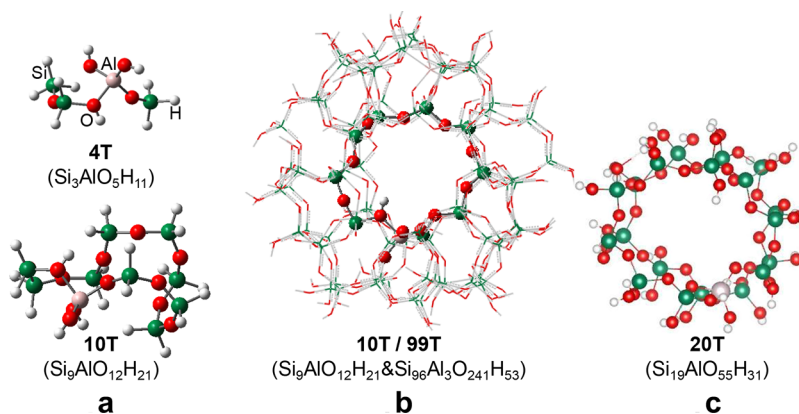
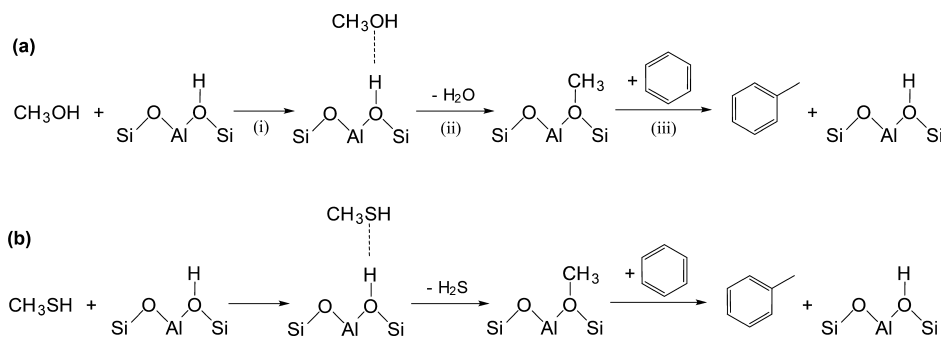
In Table 1, we summarize the results from the experimental conversion of methyl mercaptan and methanol, investigated

Table 1. Methyl Mercaptan and Methanol Conversion over H-ZSM-5 at 823 K<sup>†</sup>

process/reagent	conversion <sup>a</sup> , %	selectivity to products <sup>b</sup> , %			
		C1–C3 <sup>c</sup>	BTX <sup>d</sup>	olefins	coke
M2TH/ $\text{CH}_3\text{SH}$	>97	52	40	<0.5	7.7
MTH/ $\text{CH}_3\text{OH}$	>99	15	46	37	2.0

<sup>a</sup>Average value over 10 h on stream. <sup>b</sup>Defined as (carbon in products)/(carbon converted from  $\text{CH}_3\text{SH}$ )  $\times 100$ . <sup>c</sup> $\text{CH}_4 + \text{C}_2\text{H}_6 + \text{C}_3\text{H}_8$ . <sup>d</sup>Benzene + toluene + xylene. Conditions:  $T = 823 \text{ K}$ , WHSV =  $0.30 \text{ h}^{-1}$ .

under equivalent conditions: 823 K, WHSV =  $0.30 \text{ h}^{-1}$  over H-ZSM-5 as the catalyst,<sup>4</sup> reporting the percentage of conversion and amount of products formed during conversion. These results reveal that catalyst lifetime and product distribution constitute the principal differences between M2TH and MTH. In the M2TH process, mercaptan conversion remains at 99% for 8 h, before decreasing smoothly to 75% after 17 h of operation.<sup>4</sup> In the case of methanol conversion (the MTH

Scheme 4. Stepwise Mechanisms for the Methylation of Aromatics on Zeolites with (a) CH<sub>3</sub>OH and (b) CH<sub>3</sub>SH

**Figure 1.** Cluster models of the H-ZSM-5 pore representing 4T and 10T clusters in the gas phase (1a), embedded 10T cluster in a 99T-zeolite framework (1b) used for the geometry optimization of the reagents, intermediates, and transition states (TSs) with a two-layer ONIOM scheme, and 20T cluster in the gas phase (1c), used for the BOMD dynamics (see text for more details).

process), the catalyst exhibits enduring stability. During the first 45 h, methanol is fully converted into hydrocarbons, mainly lower olefins and aromatics.

In terms of the catalyst's lifetime, differences are associated with deactivation rates related to the amount of coke formed in each process (M2TH produces almost four times more coke than MTH) (Table 1). Concerning product distribution in the M2TH process, the main hydrocarbons that are produced are C1–C3 alkanes (with >90% of CH<sub>4</sub>) and BTX aromatics. Only very small amounts of olefins are identified among the products. Contrastingly, the MTH process produces aromatics, alkanes, and a large amount of olefins (C2–C4).

According to Scheme 1, light olefins are mainly formed during the methylation cycle of aromatics. Recently, many studies have been published discussing aromatic alkylation with methanol; these are reviewed by Ilias and Bhan.<sup>18</sup> Two reaction mechanisms have been recognized: (i) concerted mechanism, in which methanol and aromatic are coadsorbed onto a single acid site and then react in a concerted step, and (ii) stepwise mechanism, in which methanol dehydrates onto an acid site to form a surface-bound methoxide species, which then methylates aromatics by applying an Eley–Rideal-type mechanism. Theoretical studies remain inconclusive concerning which mechanism is preferable.<sup>26</sup> Spectral and kinetic experiments indicate that surface methoxide species are very likely involved as key reactive intermediates in methanol conversion and methylation processes by methanol on zeolite catalysts.<sup>27–36</sup> Accordingly, aromatic methylation follows a pathway, as depicted in Scheme 4a, where a model reaction for the methylation of benzene over H-ZSM-5 zeolite is presented. The three main steps of this mechanism are as follows: (i)

adsorption of CH<sub>3</sub>OH on a Brønsted proton; (ii) dehydration of methanol to form surface-bound methoxy species (–OCH<sub>3</sub>), and (iii) interaction of the methoxy function with an aromatic molecule in the mobile phase (adsorbed or not) to form a methylated hydrocarbon, which then desorbs from the zeolite surface.<sup>18</sup> To evaluate the alkylation capability of methyl mercaptan in this theoretical study, both methanol and methyl mercaptan were considered to be methylating agents in the stepwise mechanism of Scheme 4a,b.

In these pathways, whereas the adsorption and dehydration steps are expected to be specific for each methylating molecule, benzene methylation with analogous methoxy species should be independent of the original reactant. Therefore, the present theoretical study at  $T = 0$  K concerns the first two steps of the stepwise mechanism.

#### Adsorption of CH<sub>3</sub>OH and CH<sub>3</sub>SH on H-ZSM-5 Zeolite.

In this investigation, we used several H-ZSM-5 models of different sizes (see Figure 1) to compare the influence of model size on adsorption energies.

An embedded cluster was considered for the dehydration reaction, emulating the previously proposed models in the studies of methylation by CH<sub>3</sub>OH over acid H-ZSM-5.<sup>17,37,38</sup> The acidic Brønsted site is represented by one hydrogen atom that is bonded to oxygen at the (O<sub>surf</sub>) surface and next to Al<sup>3+</sup>. A previous theoretical study revealed that H-ZSM-5 structures with Al<sup>3+</sup> located at 24 different positions present similar stability.<sup>39</sup> Energy differences cannot be used to distinguish between various Al<sup>3+</sup> substitution positions. Therefore, Al<sup>3+</sup> location does not modify conclusions.

The adsorption of both reactants occurs by means of the H-bond formation between the zeolite surface hydrogen, H<sub>surf</sub>

and X atom, as shown in Figure 2. The computed minimum energy adsorbate structures with characteristic bond lengths are

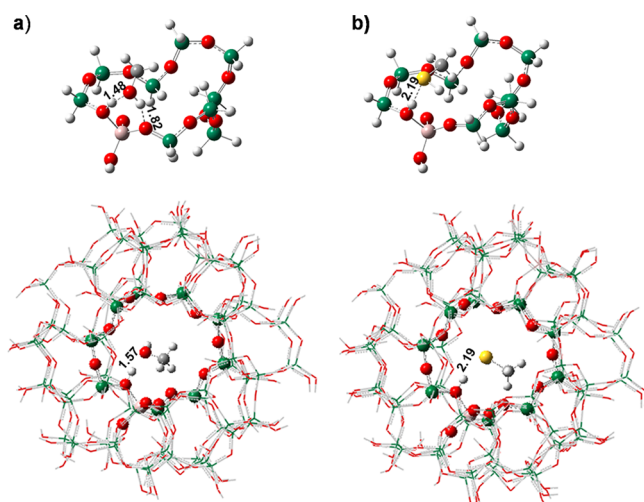


**Figure 2.** Minimum energy structures of (a) adsorbed  $\text{CH}_3\text{OH}$  and (b) adsorbed  $\text{CH}_3\text{SH}$  at the Bronsted acid site in H-ZSM-5 in the 10T (top) and embedded 10T/99T ONIOM (bottom). The reported PBE distances, being close to those computed with the other DFT functionals, are given in Å.

presented in the same figure. As expected, the methanol adsorbate geometries are characterized by shorter H bonds than the mercaptan adsorbate structures. The adsorption enthalpies and Gibbs free energies for the three zeolite models and exchange–correlation functionals are presented in Table 2.

The absolute values of the adsorption energies increase by 2–3 to 20 kcal/mol with the model size from 4T to 10T to 109T, depending on the exchange–correlation functional. M06

**Table 2.** Adsorption Energies ( $\Delta E$ ) and Thermally Corrected Gibbs Free Energies ( $\Delta G$ ) in kcal/mol of  $\text{CH}_3\text{OH}$  and  $\text{CH}_3\text{SH}$  on H-ZSM-5 Models, Computed with PBE, B3LYP, and M06 Functionals<sup>a</sup>

system	method	$\Delta E$	$\Delta G$ ( $T = 298$ K)	$\Delta G$ ( $T = 823$ K)
$\text{CH}_3\text{OH}/4\text{T}$	PBE	−22.19	−9.87	12.29
	B3LYP	−19.09	−6.70	14.31
	M06	−19.26	−6.53	12.64
$\text{CH}_3\text{SH}/4\text{T}$	PBE	−11.79	0.14	20.28
	B3LYP	−9.23	2.60	21.92
	M06	−13.09	−0.15	21.99
$\text{CH}_3\text{OH}/10\text{T}$	PBE	−25.26	−12.43	8.92
	B3LYP	−21.34	−9.62	9.75
	M06	−23.45	−8.06	14.16
$\text{CH}_3\text{SH}/10\text{T}$	PBE	−12.43	−2.92	14.25
	B3LYP	−10.76	0.52	18.57
	M06	−17.30	−2.63	18.08
$\text{CH}_3\text{OH}/10\text{T}/99\text{T}$ ONIOM	PBE	−28.18		
	B3LYP	−24.42		
	M06	−41.7		
$\text{CH}_3\text{SH}/10\text{T}/99\text{T}$ ONIOM	PBE	−17.32		
	B3LYP	−12.92		
	M06	−22.21		

<sup>a</sup>Models are included in Figure 1.

leads to a strong stabilization of mercaptan adsorption compared to Perdew, Burke, and Ernzerhof (PBE) and B3LYP results; however, in all cases, methanol adsorbate is more stable than mercaptan adsorbate by ~6 to 20 kcal/mol. This does not depend either on the theoretical method or on the model size of the zeolite.

Our  $\Delta E$  results generally coincide with previous studies on methanol adsorption.<sup>17,37,38,40</sup> The H-bond lengths of  $\text{CH}_3\text{OH}$  and  $\text{CH}_3\text{SH}$  concur with previous theoretical DFT/BLYP results,<sup>22</sup> reporting 1.52 and 2.25 Å for the  $\text{H}_{\text{surf}} \cdots \text{O}(\text{CH}_3\text{OH})$  and  $\text{H}_{\text{surf}} \cdots \text{S}(\text{CH}_3\text{SH})$  bond lengths, respectively. The methanol adsorption enthalpies are similar to the most recent theoretical studies also using the ONIOM quantum mechanics/molecular mechanics (QM/MM) approach (−24.4<sup>37</sup> and −27.4 kcal/mol<sup>16</sup>) and fall within the range of experimental methanol adsorption energies (−15 to −27 kcal/mol<sup>41,42</sup>).

The inclusion of thermal corrections and entropy contributions at  $T = 298$  K in the smallest H-ZSM-5 cluster, 1a (top), leads to  $\Delta G > 0$ , which indicates that  $\text{CH}_3\text{SH}$  is not adsorbed at the surface, represented by only a few T sites. Similarly, the  $\Delta G$  value obtained with B3LYP is positive for mercaptan/10T adsorbate. At  $T = 823$  K, positive  $\Delta G$  is found. Gibbs free energies of adsorption are not computed in the case of the 109T cluster because DFT vibrational frequency analysis is very demanding for this large size model. The differences between  $\Delta E$  and  $\Delta G$  values in Table 2 for both 4T and 10T structures at  $T = 298$  K are ~10–15 and ~20–35 kcal/mol at  $T = 823$  K, respectively, irrespective of the functional and model size.

Positive Gibbs free energy of adsorption indicates spontaneous desorption. Consequently, the adsorption reaction is not favored thermodynamically. This contradicts experimental studies that report the adsorption of methanol and methyl mercaptan on H-ZSM-5 at temperatures higher than 773 K.<sup>4</sup> It is worth noting that the thermal corrections and entropy are computed in the approximation of the ideal polyatomic gas<sup>43</sup> from the vibrational frequencies. During the last two decades, various scaling factors were proposed to correct DFT vibrational frequencies and the posteriori-derived thermodynamics quantities.<sup>44</sup> However, our calculations revealed large positive free energies of adsorption at  $T = 823$  K that cannot be corrected by scaling. This suggests that the approximation of the ideal polyatomic gas,<sup>43</sup> used in the calculations of  $\Delta G$ , fails to reproduce the experimental data for the systems and temperatures considered. Therefore, in the following, we only compare the electronic PES for both reactants with the energy barriers computed from the electronic total energies (vide infra) at  $T = 0$  K, usually referred to as “intrinsic” reaction barriers.<sup>39</sup>

**Dehydration of Methanol and Mercaptan over H-ZSM-5.** Previous theoretical studies concluded that the dehydration of methanol is an endothermic reaction with an energy barrier of ~40 kcal/mol.<sup>37,38,45</sup> We studied this using the 10/99T ONIOM model in Figure 1, as described in the “Models and Computational Details” section. The methanol transition-state (TS) structure obtained, shown in Figure 3a, closely resembles the previously described TS complex.<sup>37,38</sup> The TS complex in the mercaptan dehydration reaction, shown in Figure 3b, is characterized by a longer C–S separation compared to the C–O distance in Figure 3a. The H bonds formed with  $\text{O}_{\text{surf}}$  in the mercaptan TS are also longer than in the methanol TS structure. Similar geometric differences can be observed in the methoxy intermediate and adsorbed  $\text{H}_2\text{O}$  and  $\text{H}_2\text{S}$  geometries, presented in Figure 3c,d.



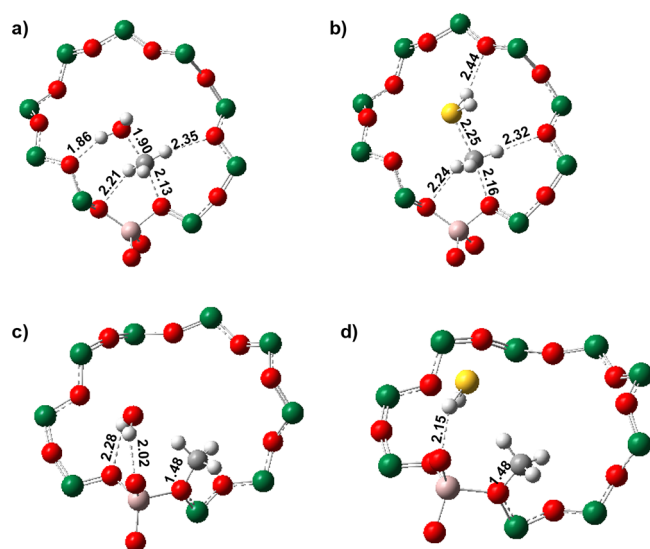


**Figure 3.** Geometries of 10T/99T ONIOM dehydration TSs of (a) methanol and (b) methyl mercaptan reagents. 10T/99T ONIOM methoxy intermediate structures (c)  $\text{CH}_3\cdots\text{H}_2\text{O}$  and (d)  $\text{CH}_3\cdots\text{H}_2\text{S}$ . Distances are given in Å.

In Figure 4, we present the PBE, B3LYP, and M06 intrinsic PES. The energy barriers, the formation energies of the methoxy intermediate ( $\text{Int\_Met}\cdots\text{H}_2\text{X}$ ), and the  $\text{H}_2\text{X}$  desorption are reported in Table 3. For methanol dehydration, the energy barriers to  $\text{Int\_Met}\cdots\text{H}_2\text{O}$  are 24.6 (PBE), 22.8 (B3LYP), and 34.8 (M06) kcal/mol. These values are smaller than the  $\sim 40$  kcal/mol intrinsic energy barrier reported previously.<sup>37,38,45</sup> We also localized TS structures with higher barriers (of  $\sim 50$  kcal/mol) and less stable methoxy intermediates, with  $\text{H}_2\text{X}$  close to the opposite site of  $\text{Al}^{3+}$  that forms H bonds with  $\text{O}_{\text{surf}}$  of  $-\text{Si}-\text{O}-\text{Si}-$  groups. These higher-energy TS geometries are shown in Figure 5. Apparently, PES has several local minima and maxima, with structures that differ mainly in the  $\text{H}_2\text{X}$  orientation and in the positions at the zeolite cavity. These small differences in TS geometries can yield TS energies that differ by several tenths of kcal/mol.

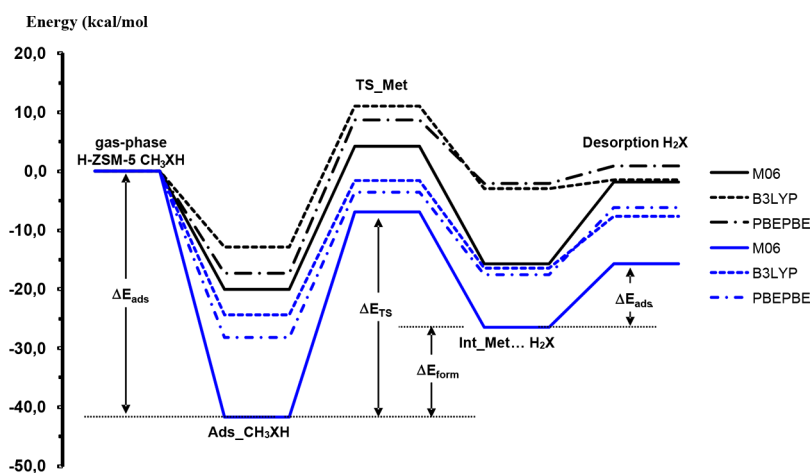


**Figure 4.** Relative energies, computed with PBE, B3LYP, and M06 DFT exchange–correlation functionals, of adsorbed  $\text{CH}_3\text{XH}$  molecules,  $\text{X} = \text{O}$  (blue lines) and  $\text{S}$  (black lines). On the  $\text{CH}_3\text{OH}$  M06 pathway, adsorption energy ( $\Delta E_{\text{ads}}$ ), reaction barrier ( $\Delta E_{\text{TS}}$ ), surface methoxy formation ( $\Delta E_{\text{form}}$ ), and  $\text{H}_2\text{O}$  desorption ( $\Delta E_{\text{desorb}}$ ) are indicated, and their values are reported in Table 3.

**Table 3.** PBE, B3LYP, and M06 Energies of the Reaction Barrier,  $\Delta E_{\text{TS}}$ , Surface Methoxy Formation,  $\Delta E_{\text{form}}$ , and Desorption of  $\text{H}_2\text{X}$ ,  $\Delta E_{\text{desorb}}$ , of  $\text{CH}_3\text{OH}/\text{CH}_3\text{SH}$  Dehydration over H-ZSM-5

	$\text{CH}_3\text{OH}$			$\text{CH}_3\text{SH}$		
	$\Delta E_{\text{TS}}$	$\Delta E_{\text{form}}$	$\Delta E_{\text{desorb}}$	$\Delta E_{\text{TS}}$	$\Delta E_{\text{form}}$	$\Delta E_{\text{desorb}}$
PBE	24.6	10.9	10.0	26.4	15.5	1.5
B3LYP	22.8	11.5	10.4	23.9	13.7	3.0
M06	34.8	15.4	13.9	26.4	6.5	10.8

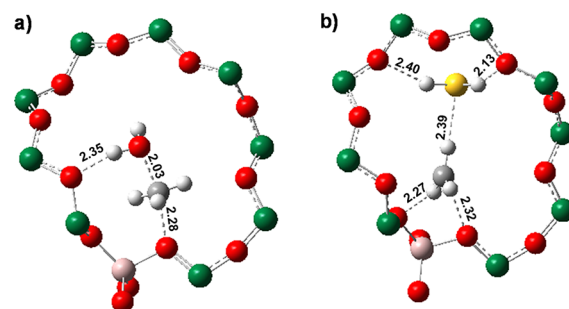


**Figure 5.** Higher-energy TS structures and characteristic geometrical parameters, localized at the PES of (a) methanol and (b) methyl mercaptan dehydration reactions, using the 10T/99T ONIOM model. Distances are given in Å.

A more significant result is that the energy barriers to the methoxy intermediate,  $\text{Int\_Met}\cdots\text{H}_2\text{X}$ , are very comparable using PBE and B3LYP functionals. In the reaction of mercaptan and methoxy intermediate, the barrier is higher by only 1.5–1.8 kcal/mol. On the contrary, the M06 functional gives an 8 kcal/mol smaller TS barrier for mercaptan versus methanol dehydration (see  $\Delta E_{\text{TS}}$  values in Table 3).

The formation energies of  $\text{Int\_Met}\cdots\text{H}_2\text{X}$  (Table 3) obtained from the equation

$$\Delta E_{\text{form}} = \Delta E(\text{Int\_Met}\cdots\text{H}_2\text{X}) - \Delta E_{\text{ads}}(\text{Ads\_CH}_3\text{XH})$$

are similar for both reagents, except with the M06 functional that reveals a nearly two times smaller  $\Delta E_{\text{form}}$  for the  $\text{CH}_3\text{SH}$  reagent, which follows from the enhanced M06 adsorption of mercaptan. After  $\text{H}_2\text{O}/\text{H}_2\text{S}$  desorption, the relative energy of

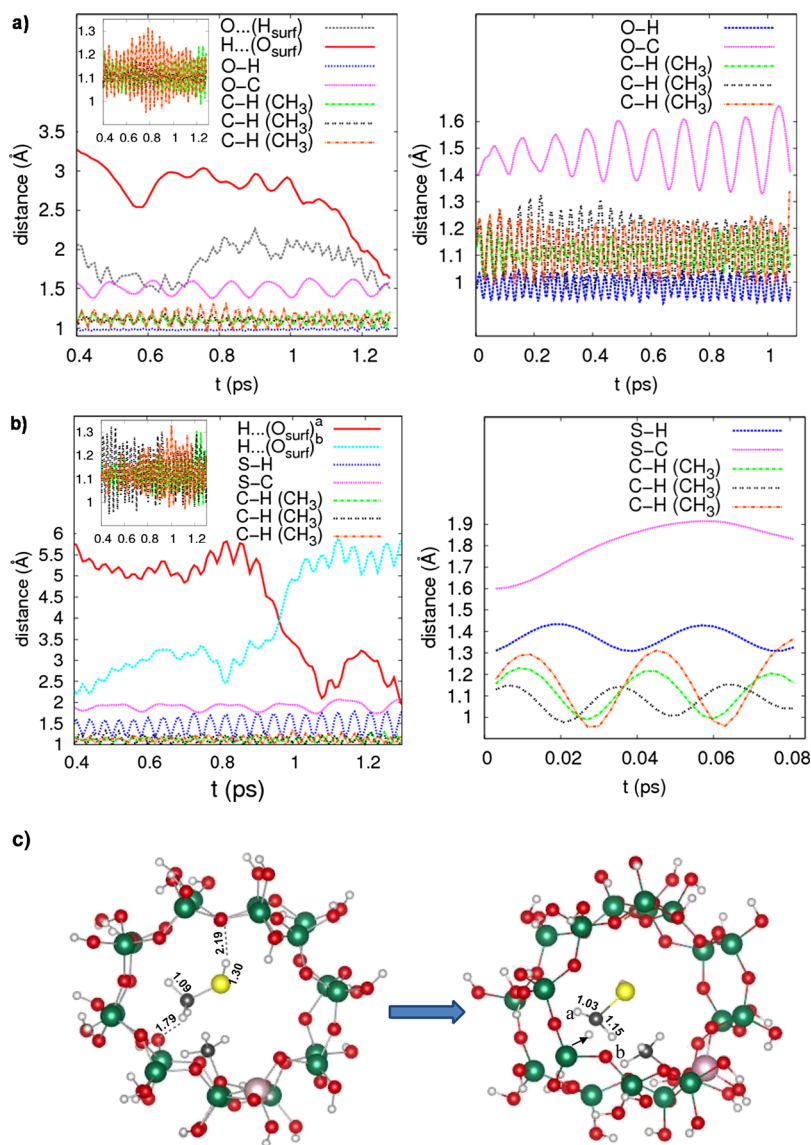


**Figure 6.** Characteristic bond lengths in Å as a function of time from the BOMD simulations of the 20T zeolite model with adsorbed (a) methanol (left panel) and coadsorbed methanol and methoxy (right panel); (b) mercaptan (left panel) and coadsorbed mercaptan and methoxy (right panel) and (c) BOMD initial (to the left of the arrow) and final (to the right of the arrow) structures of CH<sub>3</sub>SH and surface methoxy. The oxygen atoms, labeled as a and b in the right panel, are those that form H bonds with the mercaptan hydrogen.

surface methoxy resulting from the reaction with mercaptan was smaller by 5–6 kcal/mol than that formed from the methanol reagent (see Figure 4). Our computed relative energies of Int\_Met...H<sub>2</sub>O and that of surface methoxy are more negative by 5–7 kcal/mol than the previous B3LYP results.<sup>38</sup> We attribute this difference to slightly different geometrical parameters.

Although the relative energies of the adsorbate, intermediate, and products at the PES of mercaptan to the surface methoxy reaction are higher than those for the methanol reactant, the intrinsic TS barriers are very similar and even smaller for mercaptan as found with the M06 functional. This suggests that the formation of stable surface methoxy following Scheme 4 is energetically favored, immaterial of the use of methanol or methyl mercaptan reagents. Our conclusion corroborates the similarities obtained between the reaction pathways of methanol and mercaptan dehydration in chabazite,<sup>24</sup> which demonstrates that the DFT approaches and models implemented have little impact on the comparison of methanol/

mercaptan reaction pathways, despite some differences in the numerical values of the energies. Moreover, the concerted mechanism and formation of C–C bonds for both CH<sub>3</sub>XH reagents were shown to be very similar in chabazite from the static DFT reaction barriers. Therefore, we did not attempt computations of intrinsic reaction pathways for the other possible reaction mechanisms in H-ZSM-5 models because we did not anticipate any significant difference of the intrinsic energy barriers that could be useful to answer the questions of the origins for the observed very different reaction mechanisms of both reagents.

Computational results also concur with the experiments reported for both reactants concerning the formation of CH<sub>3</sub>XCH<sub>3</sub> and H<sub>2</sub>X desorption but at different temperatures, as shown in Scheme 2.<sup>2,4</sup> For the reaction with methyl mercaptan reagent to continue, an increase in temperature of up to 823 K was necessary.<sup>4</sup> A detailed explanation of mercaptan conversion at this temperature is still lacking. As mentioned previously, correction of the intrinsic PES at  $T =$

823 K by the thermodynamic quantities evaluated in the ideal polyatomic gas approximation posteriori to the DFT electronic structure calculations at  $T = 0$  K produced unrealistic positive adsorption energies and appeared inappropriate for methanol/mercaptan adsorption at high temperatures. We therefore used BOMD to account for the effect of fast rotational and vibrational motions at the experimental temperature.

**BOMD Simulations.** BOMD simulations at  $T = 823$  K were carried out on models of adsorbed methanol/mercaptan in the H-ZSM-5 cavity, as well as on structures containing surface methoxy and one  $\text{CH}_3\text{XH}$  molecule in the cavity. The former model is used to estimate the temperature effect on the adsorption process, which is the first step of the reaction, whereas the latter structure is used to model the reaction between surface methoxy and  $\text{CH}_3\text{XH}$ . According to the experimental study,<sup>4</sup> at temperatures  $< 773$  K, the only products are  $\text{CH}_3\text{SCH}_3$  and  $\text{H}_2\text{S}$  (see Scheme 2). Only after increasing the temperature to above 773 K and setting it to  $T = 823$  K in the experiments did we observe total conversion of methyl mercaptan to alkanes, BTX, and  $\text{H}_2\text{S}$ . As the intrinsic TS energy barrier (Figure 4) presents no obstacle for the mercaptan dehydration of surface methoxy, we explicitly considered the rotational and vibrational degrees of freedom along BOMD simulations. The latter are expected to provide initial information about the effect of temperature on the structural evolutions of the reagents in the zeolite cavity. The zeolite model in question is the 20T cluster in Figure 1c, and details of the dynamic simulations are provided in the “Models and Computational Details” section.

First, considering the dynamics of  $\text{CH}_3\text{XH}$  reagents at  $T = 823$  K, prior to the formation of surface methoxy, we found that both molecules adsorb at the zeolite surface via the formation and deformation of hydrogen bond(s). In the left panels in Figure 6a,b, we present the evolution of characteristic structural parameters, such as  $\text{H}_{\text{surf}} \cdots \text{O}(\text{CH}_3\text{OH})$ ;  $\text{O}_{\text{surf}} \cdots \text{H}(\text{HX}-)$ ; and X–H, X–C, and C–H bond lengths. Methanol forms the shortest H bond with its oxygen and the zeolite hydrogen at the Brønsted site. This bond length oscillates between 1.5 and 2.3 Å. Dynamic H bond(s) with surface oxygen(s) are also formed. The shortest  $\text{O}_{\text{surf}} \cdots \text{H}(\text{HO}-)$  is shown in Figure 6a, left panel. Mercaptan predominantly rotates between two surface oxygens, labeled as a and b in Figure 6b (left panel) and indicated on the 20T zeolite structure in Figure 6c. Most of the time, these two dynamic H bonds vary within an interval of 2.0–3.0 Å (Figure 6b, left). Mercaptan H (HS–) tends to dissociate as indicated by the elongation of the S–H bond; however, for the considered simulation time, mercaptan remains intact with the S–H length oscillating between 1.20 and 1.75 Å. The optimized bond length at  $T = 0$  K S–H of the adsorbed mercaptan in the ONIOM 10T/99T structure is 1.36 Å. Contrastingly, the methanol O–H distance remains very close to its optimized value of 0.99 Å. Likewise, the average bond lengths for C–O and C–S over all the snapshots are 1.51 and 1.90 Å, respectively. These values resemble the optimized respective bond distances of 1.44 Å (C–O) and 1.84 Å (C–S). The C–H distance oscillations in the range of 0.9–1.3 Å are obtained for both mercaptan and methanol along the dynamics. This analysis suggests that initially both adsorbed molecules remain intact and undergo similar structural evolution, although subsequently some differences emerge (see Figure 6a,b, left panels).

This also corroborates experimental findings, which indicate that the adsorption on the zeolite catalysts represents a first

methylation step on the reaction pathway of methanol and mercaptan (Scheme 4) at  $T = 823$  K.

The presence of surface methoxy and  $\text{CH}_3\text{XH}$  in the zeolite cavity conducted to different dynamics of  $\text{CH}_3\text{OH}$  and  $\text{CH}_3\text{SH}$ . A very fast dissociation of one methyl hydrogen occurred in mercaptan, producing a  $\bullet\text{CH}_2\text{SH}$  radical. The dissociation occurred after 83 fs simulation time and energy convergence was broken once the methyl hydrogen had dissociated because of the presence of the nonbonded abstracted H atom. The important bond distances in the initial and final snapshot structure are reported in Figure 6c. The C–H and X–C bond evolution along the dynamics are presented in the right panels in Figure 6a,b. The C–X bond length variations remain similar to the isolated adsorbed molecules in the cavity. Elongation of one C–H distance  $\geq 1.34$  Å causes hydrogen abstraction. A similar effect of hydrogen abstraction from the methyl group in  $\text{CH}_3\text{OH}$  is established when  $\text{CH}_3\text{OH}$  is adsorbed in the presence of surface methoxy, but this process is roughly 10 times slower than the H dissociation from the coadsorbed methyl mercaptan molecule.

To verify the BOMD results, we repeated the simulations of mercaptan and surface methoxy in the 20T zeolite cluster with larger bases, TZVP, and without constraining the cluster geometry. The  $\bullet\text{CH}_2\text{SH}$  radical is again obtained after a somewhat longer simulation time of 210 fs. Therefore, larger bases would systematically slow down the processes but with no effect on the resulting trends.

Rapid formation of  $\bullet\text{CH}_2\text{SH}$  radical from mercaptan in a water solvent was reported previously in electron spin resonance studies.<sup>46</sup> This process was explained with reference to the constraint of free methyl rotation around the C–S bond by the hydrogen bonds between mercaptan and the oxygen of  $\text{H}_2\text{O}$ . Hindered rotation was thought to induce a nonequivalent orbital coupling between the atomic orbitals of carbon and the three hydrogen atoms in the  $\text{CH}_3$  group. This promotes coupling between only one or two C–H atoms and causes very rapid dissociation from  $-\text{CH}_3$  on the part of the remaining hydrogen.<sup>47</sup> The latter process is known as hydrogen abstraction. An analogous mechanism has been suggested for the formation of  $\text{CH}_3\text{S}^\bullet$  and  $\bullet\text{CH}_3$  radicals. Similar to mercaptan in water solvent, C–S rotation is hindered in the zeolite cavity because of the formation of hydrogen bonds between the methyl  $\text{H} \cdots \text{O}_{\text{surf}}$  and  $\text{H}(\text{HS}) \cdots \text{O}_{\text{surf}}$  (see Figure 6c). In the initial geometry of the coadsorbed  $\text{CH}_3\text{SH}$  molecule, the three C–H distances are identical, equal to 1.09 Å. In the final snapshot structure in Figure 6c with the  $\bullet\text{CH}_2\text{SH}$  radical, to the right of the arrow, one C–H distance is shorter, 1.03 Å, and the other two are 1.15 and 1.34 Å. The C–H bonds oscillate between comparable values in the isolated adsorbed molecules (inset in the left panels in Figure 6a,b) without exceeding the dissociation limit of  $\text{C–H} \geq 1.34$  Å. The very fast hydrogen abstraction from the methyl group in  $\text{CH}_3\text{SH}$  therefore most likely refers to an increase in constraint caused by mercaptan in the presence of surface methoxy. The high reaction temperature seems to favor hydrogen abstraction from the methyl group in mercaptan but not from the S–H group. It cannot be ruled out that other initial geometries may produce other radicals such as  $\text{CH}_3\text{X}^\bullet$ . The very complex kinetics in the proposed hydrogen pool mechanism<sup>8–12</sup> may thus be associated with various speeds and natures of radicals, formed under particular experimental conditions.

One can speculate that the competition between hydrogen abstraction and the C–C bond formation at a given



temperature is likely to be the predominant factor determining the reactivity of methanol and mercaptan, as well as the rate of coke deposition poisoning the catalyst. Other mechanisms could also be envisaged. A more thorough quantitative biased dynamics study of the free-energy profiles is necessary and will be a subject of future work. Various biased dynamics techniques, such as umbrella sampling<sup>48</sup> or perturbation MD,<sup>49</sup> coupled to QM/MM have been successfully used to unveil catalytic mechanisms at finite temperatures. On the basis of experiments, the occurrence of radical decomposition reactions and hydrogen abstraction was apparent in the mechanism involving the conversion of methanol and mercaptan to ethylene over acidic  $\text{WO}_3/\text{g-Al}_2\text{O}_3$  catalysts at  $T > 327$  C, studied by Olah et al.<sup>50</sup> In the latter work, the formation of methane as a byproduct was associated with the thermal decomposition of dimethylether ( $\text{CH}_3\text{OCH}_3 \rightarrow \text{CH}_4 + \text{CH}_2\text{O}$ ).

The present study demonstrates that the differences in the conversion of mercaptan and methanol over acid zeolite catalysts are not related to the electronic structures of  $\text{CH}_3\text{SH}$  and  $\text{CH}_3\text{OH}$  and the intrinsic pathways. Instead, these differences are determined by the speed and type of radicals arising from  $\text{CH}_3\text{SH}/\text{CH}_3\text{OH}$  molecules with constrained motions in the zeolite cavity, where surface methoxy is found.

## CONCLUSIONS

DFT and BOMD were employed to compare methylation reactions by methanol and methyl mercaptan reagents, to reveal the underlying origins of the experimentally established differences between MTH and M2TH processes. For this purpose, we studied the intrinsic PES in the stepwise mechanism and the role of fast rotational and vibrational motions for both reagents.

The DFT intrinsic PESs of the dehydration reactions of  $\text{CH}_3\text{XH}$  to surface methoxy do not exhibit any conclusive difference, from which to distinguish between methanol and mercaptan.

BOMD simulations at the experimental temperature (823 K) and the analysis of the evolution of molecular bonds reveal initial intact adsorbate structures for the  $\text{CH}_3\text{OH}$  and  $\text{CH}_3\text{SH}$  molecules. The dynamics of methyl mercaptan adsorbed in the cavity with surface methoxy led to the formation of  $\bullet\text{CH}_2\text{SH}$  radical. A similar phenomenon occurred for the coadsorbed methanol and the surface methoxy but after a simulation period of 10 times the length. Hydrogen abstraction from methanol and mercaptan in zeolites can be attributed to the hindered C–X rotation because of the  $\text{H}(\text{CH}_3)\cdots\text{O}_{\text{surf}}$  and  $\text{H}(\text{XH})\cdots\text{O}_{\text{surf}}$  hydrogen bonds, analogously to the reported hydrogen abstraction from the  $-\text{CH}_3$  groups in  $\text{CH}_3\text{XH}$  dissolved in water. Following our DFT static and BOMD (at  $T = 823$  K) results, it is most probable that the different products observed experimentally from MTH and M2TH processes will relate to the different rate of radical formation under these experimental conditions.

## MODELS AND COMPUTATIONAL DETAILS

The first two gas-phase 4T and 10T models in Figure 1a are used to compute adsorption energies using DFT methods for the fully optimized structures. The dangling bonds in these clusters are saturated with H atoms. The adsorbate ground-state geometries are confirmed by vibrational frequency analysis. Computed vibrational frequencies are also used to

obtain thermal and entropy contributions to the Gibbs free energies of adsorption,  $\Delta G$ , for  $T \neq 0$  in the ideal polyatomic gas model.<sup>43</sup> Zero-point energy corrections are included in the free energies.

The third 10T/99T model in Figure 1b contains a 10T cluster ( $\text{Si}_9\text{AlO}_{12}\text{H}_{21}$ ), embedded in a 99T-zeolite framework ( $\text{Si}_{96}\text{Al}_3\text{O}_{241}\text{H}_{53}$ ). The inner  $\text{Si}_9\text{AlO}_{12}\text{H}_{21}$  cluster is treated at the DFT level and the remaining 99T structure is described with the United Force Field (UFF)<sup>51</sup> by using the ONIOM (our own N-layered integrated molecular orbital and molecular mechanics)<sup>52–55</sup> with the embedded QM/MM scheme. This is used to optimize the minima and maxima structures at the PES of  $\text{CH}_3\text{XH}$  dehydration reactions. The vibrational frequency computation needed to confirm the minima and the maxima at the PES is also obtained using the ONIOM scheme. We used the two-layer ONIOM scheme with electronic embedding<sup>56</sup> and carried out full geometry optimization of both the QM and MM regions.<sup>57</sup> The energies of those optimized with ONIOM structures are subsequently computed at the DFT level that was applied to the entire 109T optimized structures. This approach was employed to avoid inaccurate energy calculations from the molecular UFF in the ONIOM embedding scheme.<sup>38</sup>

The above-described calculations were carried out with Gaussian 09 program<sup>58</sup> with three exchange–correlation DFT functionals that are the PBE,<sup>59</sup> the hybrid B3LYP functional,<sup>60,61</sup> and M06.<sup>62</sup> The atomic wave functions were described with a double-zeta quality basis set, 6-31G(d,p). In all the calculations, the energy convergence was set up to  $10^{-8}$  au. The Berny<sup>63</sup> optimization was used for the localization of the minima, intermediate, and TS structures. The convergence was based on the root-mean-square forces and displacement vectors with a threshold of  $3.0 \times 10^{-4}$  and  $1.2 \times 10^{-3}$ , respectively.

There is a fourth model named 20T cluster in Figure 1c that is used in the BOMD calculations, coupled with DFT augmented with an empirical dispersion (DFT-D) method as implemented in deMon2k program.<sup>64–67</sup> This approach was employed to study the adsorption processes of  $\text{CH}_3\text{XH}$  in H-ZSM-5, before and after the formation of surface methoxy at the experimental temperature.<sup>2</sup> The 20T cluster is cut from the optimized (with ONIOM scheme) 109T geometry (vide supra), and the dangling bonds are saturated with hydrogens. For the simulations, the outermost O–H bonds are constrained to the optimized geometry with ONIOM values. In the BOMD simulations, the temperature of the system set to 823 K was maintained using the Berendsen thermostat ( $\tau = 0.02$  ps) in the NVT ensemble. The velocity Verlet algorithm with a time step of 0.1 fs was employed. The linear and the angular momenta were conserved with a threshold of  $10^{-8}$ ; therefore, the studied systems are not allowed to translate and rotate.

## AUTHOR INFORMATION

### Corresponding Author

\*E-mail: tzonka.mineva@enscm.fr. Phone: +33467163468. Fax: +33467163470 (T.M.).

### ORCID

Tzonka Mineva: 0000-0002-9156-2396

### Notes

The authors declare no competing financial interest.



## ACKNOWLEDGMENTS

Part of the calculations was performed at the HPC resources of TGCC-CURIE under the allocation x2016087369 made by GENCI (Grand Equipement National de Calcul Intensif). This study was also funded by DGAPA-PAPIIT, Consejo Nacional de Ciencia y Tecnología (CONACyT), and resources were provided by the Instituto de Investigaciones en Materiales (IIM). This work was carried out using a NES supercomputer, provided by Dirección General de Cómputo y Tecnologías de Información y Comunicación (DGTIC), Universidad Nacional Autónoma de México (UNAM). M.R. and A.M. would like to thank the DGTIC of UNAM for their excellent and free supercomputing services. M.R. thanks CONACyT for the PhD scholarship (387687) and CEP.

## REFERENCES

- Huguet, E.; Coq, B.; Durand, R.; Leroi, C.; Cadours, R.; Hulea, V. A highly efficient process for transforming methyl mercaptan into hydrocarbons and H<sub>2</sub>S on solid acid catalysts. *Appl. Catal., B* **2013**, *134–135*, 344–348.
- Cammarano, C.; Huguet, E.; Cadours, R.; Leroi, C.; Coq, B.; Hulea, V. Selective transformation of methyl and ethyl mercaptans mixture to hydrocarbons and H<sub>2</sub>S on solid acid catalysts. *Appl. Catal., B* **2014**, *156–157*, 128–133.
- Tian, P.; Wei, Y.; Ye, M.; Liu, Z. Methanol to Olefins (MTO): from fundamentals to commercialization. *ACS Catal.* **2015**, *5*, 1922–1938.
- Hulea, V.; Huguet, E.; Cammarano, C.; Lacarriere, A.; Durand, R.; Leroi, C.; Cadours, R.; Coq, B. Conversion of methyl mercaptan and methanol to hydrocarbons over solid acid catalysts—a comparative study. *Appl. Catal., B* **2014**, *144*, 547–553.
- Butter, S. A.; Jurewicz, A. T.; Kaeding, W. W. Conversion of alcohols, mercaptans, sulfides, halides and/or amines. U.S. Patent 3,894,107, July 8, 1975.
- Wachs, E. Production of hydrocarbons from mercaptans. U.S. Patent 20,030,060,672, Mar 23, 2003.
- Mashkina, A. V.; Grunvald, V. R.; Nasteka, V. I.; Borodin, B. P.; Yakovleva, V. N.; Khairulina, L. N. Decomposition of alkanethiols to dialkyl sulfides and hydrogen sulfide. *React. Kinet. Catal. Lett.* **1990**, *41*, 357–362.
- Dessau, R. M. On the H-ZSM-5 catalyzed formation of ethylene from methanol or higher olefins. *J. Catal.* **1986**, *99*, 111–116.
- Dahl, I. M.; Kolboe, S. On the reaction mechanism for propene formation in the MTO reaction over SAPO-34. *Catal. Lett.* **1993**, *20*, 329–336.
- Stöcker, M. Methanol-to-hydrocarbons: catalytic materials and their behavior. *Microporous Mesoporous Mater.* **1999**, *29*, 3–48.
- Haw, J. F.; Song, W.; Marcus, D. M.; Nicholas, J. B. The mechanism of methanol to hydrocarbon catalysis. *Acc. Chem. Res.* **2003**, *36*, 317–326.
- Bjorgen, M.; Svelle, S.; Joensen, F.; Nerlov, J.; Kolboe, S.; Bonino, F.; Palumbo, L.; Bordiga, S.; Olsbye, U. Conversion of methanol to hydrocarbons over zeolite H-ZSM-5: On the origin of the olefinic species. *J. Catal.* **2007**, *249*, 195–207.
- Wei, Y.; Zhang, D.; Liu, Z.; Su, B.-L. Highly efficient catalytic conversion of chloromethane to light olefins over HSAPO-34 as studied by catalytic testing and in situ FTIR. *J. Catal.* **2006**, *238*, 46–57.
- Svelle, S.; Kolboe, S.; Olsbye, U.; Swang, O. A Theoretical investigation of the methylation of methylbenzenes and alkenes by halomethanes over acidic zeolites. *J. Phys. Chem. B* **2003**, *107*, 5251–5260.
- Li, J.; Wei, Y.; Chen, J.; Tian, P.; Su, X.; Xu, S.; Qi, Y.; Wang, Q.; Zhou, Y.; He, Y.; Liu, Z. Observation of heptamethylbenzenium cation over SAPO-type molecular sieve DNL-6 under real MTO conversion conditions. *J. Am. Chem. Soc.* **2012**, *134*, 836.
- Svelle, S.; Tuma, C.; Rozanska, X.; Kerber, T.; Sauer, J. Quantum chemical modeling of zeolite-catalyzed methylation reactions: Toward chemical accuracy for barriers. *J. Am. Chem. Soc.* **2009**, *131*, 816–825.
- Van der Mynsbrugge, J.; Visur, M.; Olsbye, U.; Beato, P.; Bjorgen, M.; Van Speybroeck, V.; Svelle, S. Methylation of benzene by methanol: Single-site kinetics over H-ZSM-5 and H-beta zeolite catalysts. *J. Catal.* **2012**, *292*, 201–212.
- Ilias, S.; Bhan, A. Mechanism of the catalytic conversion of methanol to hydrocarbons. *ACS Catal.* **2013**, *3*, 18–31.
- Svelle, S.; Rønning, P. O.; Olsbye, U.; Kolboe, S. Kinetic studies of zeolite-catalyzed methylation reactions. Part 2. Co-reaction of [<sup>12</sup>C]propene or [<sup>12</sup>C]n-butene and [<sup>13</sup>C]methanol. *J. Catal.* **2005**, *234*, 385–400.
- Svelle, S.; Aravinthan, S.; Bjorgen, M.; Lillerud, K.-P.; Kolboe, S.; Dahl, I. M.; Olsbye, U. The methyl halide to hydrocarbon reaction over H-SAPO-34. *J. Catal.* **2006**, *241*, 243–254.
- Kong, L.; Shen, B. Theoretical study of the geminal methylation of methylbenzene by halomethane over HSAPO-34 molecular sieve. *Chin. J. Catal.* **2015**, *36*, 1017–1022.
- Soscún, H.; Castellano, O.; Hernández, J. Adsorption of CH<sub>3</sub>SH in acidic zeolites: A theoretical study. *J. Phys. Chem. B* **2004**, *108*, 5620–5626.
- Lü, R.; Qiu, G.; Liu, C. Density functional investigation of methanethiol and dimethyl sulfide adsorption on zeolite. *J. Nat. Gas Chem.* **2006**, *15*, 134–143.
- Baltrusaitis, J.; Bučko, T.; Michaels, W.; Makkee, M.; Mul, G. Catalytic methyl mercaptan coupling to ethylene in chabazite: DFT study of the first C–C bond formation. *Appl. Catal., B* **2016**, *187*, 195–203.
- Chang, C. D.; Silvestri, A. J. The conversion of methanol and other O-compounds to hydrocarbons over zeolite catalysts. *J. Catal.* **1977**, *47*, 249–259.
- Svelle, S.; Visur, M.; Olsbye, U.; Saepurahman; Bjorgen, M. Mechanistic aspects of the zeolite catalyzed methylation of alkenes and aromatics with methanol: A review. *Top. Catal.* **2011**, *54*, 897–906.
- Forester, T. R.; Howe, R. F. In Situ FTIR Studies of Methanol and Dimethyl Ether in ZSM-5. *J. Am. Chem. Soc.* **1987**, *109*, 5076–5082.
- Cheung, P.; Bhan, A.; Sunley, G. J.; Law, D. J.; Iglesia, E. Site requirements and elementary steps in dimethyl ether carbonylation catalyzed by acidic zeolites. *J. Catal.* **2007**, *245*, 110–123.
- Yamazaki, H.; Shima, H.; Imai, H.; Yokoi, T.; Tatsumi, T.; Kondo, J. N. Evidence for a “carbene-like” intermediate during the reaction of methoxy species with light alkenes on H-ZSM-5. *Angew. Chem., Int. Ed.* **2011**, *50*, 1853–1856.
- Song, W.; Haw, J. F.; Nicholas, J. B.; Heneghan, C. S. Methylbenzenes are the organic reaction centers for methanol-to-olefin catalysis on HSAPO-34. *J. Am. Chem. Soc.* **2000**, *122*, 10726–10727.
- Bosacek, V. Formation of surface-bonded methoxy groups in the sorption of methanol and methyl iodide on zeolites studied by carbon-13 MAS NMR spectroscopy. *J. Phys. Chem.* **1993**, *97*, 10732–10737.
- Wang, W.; Buchholz, A.; Seiler, M.; Hunger, M. Evidence for an initiation of the methanol-to-olefin process by reactive surface methoxy groups on acidic zeolite catalysts. *J. Am. Chem. Soc.* **2003**, *125*, 15260–15267.
- Wang, W.; Hunger, M. Reactivity of surface alkoxy species on acidic zeolite catalysts. *Acc. Chem. Res.* **2008**, *41*, 895–904.
- Jiang, Y.; Hunger, M.; Wang, W. On the reactivity of surface methoxy species in acidic zeolites. *J. Am. Chem. Soc.* **2006**, *128*, 11679–11692.
- Mirth, G.; Lercher, J. A. Co-adsorption of toluene and methanol on HZSM-5 zeolites. *J. Phys. Chem.* **1991**, *95*, 3736–3740.
- Broggaard, R. Y.; Henry, R.; Schuurman, Y.; Medford, A. J.; Moses, P. G.; Beato, P.; Svelle, S.; Nørskov, J. K.; Olsbye, U. Methanol-to-hydrocarbons conversion: The alkene methylation pathway. *J. Catal.* **2014**, *314*, 159–169.

- (37) Maihom, T.; Boekfa, B.; Sirijaraensre, J.; Nanok, T.; Probst, M.; Limtrakul, J. Reaction mechanisms of the methylation of ethene with methanol and dimethyl ether over H-ZSM-5: An ONIOM study. *J. Phys. Chem. C* **2009**, *113*, 6654–6662.
- (38) Nie, X.; Janik, M. J.; Guo, X.; Song, G. Shape-selective methylation of 2-methylnaphthalene with methanol over H-ZSM-5 zeolite: A computational study. *J. Phys. Chem. C* **2012**, *116*, 4071–4082.
- (39) Sklenak, S.; Dědeček, J.; Li, C.; Wichterlová, B.; Gábová, V.; Sierka, M.; Sauer, J. Aluminum siting in silicon-rich zeolite frameworks: A combined high-resolution  $^{27}\text{Al}$  NMR spectroscopy and quantum mechanics/molecular mechanics study of ZSM-5. *Angew. Chem.* **2007**, *119*, 7424–7427.
- (40) Hansen, N.; Brüggemann, T.; Bell, A. T.; Keil, F. J. Theoretical investigation of benzene alkylation with ethene over H-ZSM-5. *J. Phys. Chem. C* **2008**, *112*, 15402–15411.
- (41) Lee, C.-C.; Gorte, R. J.; Farneth, W. E. Calorimetric Study of Alcohol and Nitrile Adsorption Complexes in H-ZSM-5. *J. Phys. Chem. B* **1997**, *101*, 3811–3817.
- (42) Messow, U.; Quitzsch, K.; Herden, H. Heats of immersion of ZSM-5 zeolite in n-alkanes, 1-alkenes and 1-alcohols at 30°C. *Zeolites* **1984**, *4*, 255–258.
- (43) McQuarrie, D. A. *Statistical Thermodynamics*, 1st ed.; Harper and Row: New York, 1973; Chapter 8.
- (44) Merrick, J. P.; Moran, D.; Radom, L. An evaluation of harmonic vibrational frequency scale factors. *J. Phys. Chem. A* **2007**, *111*, 11683–11700.
- (45) Jansang, B.; Nanok, T.; Limtrakul, J. Structure and reaction mechanism of alkylation of phenol with methanol over H-FAU zeolite: An ONIOM study. *J. Phys. Chem. C* **2008**, *112*, 540–547.
- (46) Volman, D. H.; Wolstenholme, J.; Hadley, S. G. Photochemical formation of free radical from hydrogen sulfide, mercaptans, and cysteine. *J. Phys. Chem.* **1967**, *71*, 1798–1803.
- (47) Kurita, Y.; Gordy, W. Electron spin resonance in a gamma-irradiated single crystal of L-cystine dihydrochloride. *J. Chem. Phys.* **1961**, *34*, 282–288.
- (48) Liu, X.; Salahub, D. R. Molybdenum Carbide Nanocatalysts at Work in the in Situ Environment: A Density Functional Tight-Binding and Quantum Mechanical/Molecular Mechanical Study. *J. Am. Chem. Soc.* **2015**, *137*, 4249–4259.
- (49) Wang, L.; Broyde, S.; Zhang, Y. Polymerase-Tailored Variations in the Water-Mediated and Substrate-Assisted Mechanism for Nucleotidyl Transfer: Insights from a Study of T7 DNA Polymerase. *J. Mol. Biol.* **2009**, *389*, 787–796.
- (50) Olah, G. A.; Doggweiler, H.; Felberg, J. D.; Frohlich, S.; Grdina, M. J.; Karpeles, R.; Keumi, T.; Inaba, S.-I.; Ip, W. M.; Lammertsma, K.; Salem, G.; Tabor, D. Onium ylide chemistry. 1. Bifunctional acid-base-catalyzed conversion of heterosubstituted methanes into ethylene and derived hydrocarbons. The onium ylide mechanism of the  $\text{C}_1 \rightarrow \text{C}_2$  conversion. *J. Am. Chem. Soc.* **1984**, *106*, 2143–2149.
- (51) Rappe, A. K.; Casewit, C. J.; Colwell, K. S.; Goddard, W. A.; Skiff, W. M. UFF, a full periodic table force field for molecular mechanics and molecular dynamics simulations. *J. Am. Chem. Soc.* **1992**, *114*, 10024–10035.
- (52) Maseras, F.; Morokuma, K. IMOMM: A new integrated *ab initio* + molecular mechanics geometry optimization scheme of equilibrium structures and transition states. *J. Comput. Chem.* **1995**, *16*, 1170–1179.
- (53) Humbel, S.; Sieber, S.; Morokuma, K. The IMOMO method: Integration of different levels of molecular orbital approximations for geometry optimization of large systems: Test for *n*-butane conformation and  $\text{SN}_2$  reaction:  $\text{RCl} + \text{Cl}^-$ . *J. Chem. Phys.* **1996**, *105*, 1959–1967.
- (54) Svensson, M.; Humbel, S.; Morokuma, K. Energetics using the single point IMOMO (integrated molecular orbital+molecular orbital) calculations: Choices of computational levels and model system. *J. Chem. Phys.* **1996**, *105*, 3654–3661.
- (55) Svensson, M.; Humbel, S.; Froese, R. D. J.; Matsubara, T.; Sieber, S.; Morokuma, K. ONIOM: A multilayered integrated MO + MM method for geometry optimizations and single point energy predictions. A test for Diels–Alder reactions and  $\text{Pt}(\text{P}(t\text{-Bu})_3)_2 + \text{H}_2$  oxidative addition. *J. Phys. Chem.* **1996**, *100*, 19357–19363.
- (56) Vreven, T.; Byun, K. S.; Komáromi, I.; Dapprich, S.; Montgomery, J. A., Jr.; Morokuma, K.; Frisch, M. J. Combining quantum mechanics methods with molecular mechanics methods in ONIOM. *J. Chem. Theory Comput.* **2006**, *2*, 815–826.
- (57) Vreven, T.; Frisch, M. J.; Kudin, K. N.; Schlegel, H. B.; Morokuma, K. Geometry optimization with QM/MM methods II: Explicit quadratic coupling. *Mol. Phys.* **2006**, *104*, 701–714.
- (58) Frisch, M. J.; Trucks, G. W.; Schlegel, H. B.; Scuseria, G. E.; Robb, M. A.; Cheeseman, J. R.; Scalmani, G.; Barone, V.; Mennucci, B.; Petersson, G. A.; Nakatsuji, H.; Caricato, M.; Li, X.; Hratchian, H. P.; Izmaylov, A. F.; Bloino, J.; Zheng, G.; Sonnenberg, J. L.; Hada, M.; Ehara, M.; Toyota, K.; Fukuda, R.; Hasegawa, J.; Ishida, M.; Nakajima, T.; Honda, Y.; Kitao, O.; Nakai, H.; Vreven, T.; Montgomery, J. A., Jr.; Peralta, J. E.; Ogliaro, F.; Bearpark, M.; Heyd, J. J.; Brothers, E.; Kudin, K. N.; Staroverov, V. N.; Kobayashi, R.; Normand, J.; Raghavachari, K.; Rendell, A.; Burant, J. C.; Iyengar, S. S.; Tomasi, J.; Cossi, M. R.; Millam, N. J.; Klene, M.; Knox, J. E.; Cross, J. B.; Bakken, V.; Adamo, C.; Jaramillo, J.; Gomperts, R. E.; Stratmann, O.; Yazyev, A. J.; Austin, R.; Cammi, C.; Pomelli, J. W.; Ochterski, R.; Martin, R. L.; Morokuma, K.; Zakrzewski, V. G.; Voth, G. A.; Salvador, P.; Dannenberg, J. J.; Dapprich, S.; Daniels, A. D.; Farkas, O.; Foresman, J. B.; Ortiz, J. V.; Cioslowski, J.; Fox, D. J. *Gaussian 09*, Revision A.08; Gaussian, Inc.: Wallingford CT, 2009.
- (59) Perdew, J. P.; Burke, K.; Ernzerhof, M. Generalized gradient approximation made simple. *Phys. Rev. Lett.* **1996**, *77*, 3865–3868.
- (60) Becke, A. D. Density-functional thermochemistry. III. The role of exact exchange. *J. Chem. Phys.* **1993**, *98*, 5648–5652.
- (61) Lee, C.; Yang, W.; Parr, R. G. Development of the Colle-Salvetti correlation-energy formula into a functional of the electron density. *Phys. Rev. B: Condens. Matter Mater. Phys.* **1988**, *37*, 785–789.
- (62) Zhao, Y.; Truhlar, D. G. The M06 suite of density functionals for main group thermochemistry, thermochemical kinetics, non-covalent interactions, excited states, and transition elements: two new functionals and systematic testing of four M06-class functionals and 12 other functionals. *Theor. Chem. Acc.* **2008**, *120*, 215.
- (63) Schlegel, H. B. Optimization of equilibrium geometries and transition structures. *J. Comput. Chem.* **1982**, *3*, 214–218.
- (64) Köster, A. M.; Geudtner, G.; Alvarez-Ibarra, A.; Calaminici, P.; Casida, M. E.; Carmona-Espindola, J.; Dominguez, V.; Flores-Moreno, R.; Gamboa, G. U.; Goursot, A.; Heine, T.; Ipatov, A.; de la Lande, A.; Janetzko, F.; del Campo, J. M.; Reveles, J. U.; Vasquez-Perez, J. M.; Vela, A.; Zuniga-Gutierrez, B.; Salahub, D. R. *deMon2k*, Version 4.2.0; The deMon Developers, Cinvestav: Mexico City, 2013.
- (65) Geudtner, G.; Calaminici, P.; Carmona-Espindola, J.; del Campo, J. M.; Dominguez-Soria, V. D.; Moreno, R. F.; Gamboa, G. U.; Goursot, A.; Köster, A. M.; Reveles, J. U.; Mineva, T.; Vasquez-Pérez, J. M.; Vela, A.; Zúñiga-Gutierrez, B.; Salahub, D. R. *deMon2k*. *Wiley Interdiscip. Rev.: Comput. Mol. Sci.* **2012**, *2*, 548–555.
- (66) Godbout, N.; Salahub, D. R.; Andzelm, J.; Wimmer, E. Optimization of Gaussian-type basis sets for local spin density functional calculations. Part I. Boron through neon, optimization technique and validation. *Can. J. Chem.* **1992**, *70*, 560–571.
- (67) Köster, A. M. Hermite Gaussian auxiliary functions for the variational fitting of the Coulomb potential in density functional methods. *J. Chem. Phys.* **2003**, *118*, 9943–9951.